

Spatio-Temporal Δ - Σ N^2 -port ADC Noise Shaping for $N \times N$ Antenna Arrays

H. Malavipathirana*, A. Madanayake*, C. Edussooriya[†], S. Mandal[‡], N. Udayanga*, J. Liang[‡], L. Belostotski[§]

*Electrical and Computer Engineering, Florida International University, Email: hmala005@fiu.edu

[†]Electronic & Telecommunication Engineering, University of Moratuwa, Email: chamira@uom.lk

[‡]Electrical, Computer, and Systems Engineering, Case Western Reserve University, Email: sxm833@case.edu

[§]Electrical and Computer Engineering, University of Calgary, Email: lbelosto@ucalgary.ca

Abstract—A multi-port spatio-temporal noise-shaping ADC is proposed to process plane waves received by spatially-oversampled antenna arrays. In the proposed multi-port ADC, the desired plane waves are processed with a spatial low-pass frequency response whereas the noise and distortion are shaped with a spatial high-pass frequency response. By employing a first-order Butterworth filter, approximately circular passbands and stopbands are achieved for the signal and the noise transfer functions, respectively. The proposed noise-shaping system is designed in the TSMC 180 nm CMOS process, with ADCs and DACs modeled as noise sources. Circuit simulation results show that the proposed system can achieve a bandwidth of 50 MHz.

I. INTRODUCTION

The concept of multi-dimensional delta-sigma (Δ - Σ) noise-shaping for array receivers has recently drawn much attention [1]–[9]. The general idea is to exploit noise- and distortion-shaping in the spatio-temporal domain such that undesired noise/distortion added by the receiver can be shaped outside the region of interest of the desired signals (incoming plane waves), thus improving receiver performance metrics such as linearity, noise figure (NF), and effective number of bits (ENOB). In particular, N -port low-noise-amplifiers (LNAs) and analog-to-digital converters (ADCs) using two-dimensional (2-D) (space, time) Δ - Σ noise-shaping have been simulated in 65 nm CMOS [4], [5]. A complete CMOS array receiver using first-order spatio-temporal noise-shaping within both the LNA and ADC has also been reported in [6].

We now extend this method to multiple spatial and temporal dimensions for 2-D array receivers, and propose three-dimensional (3-D) signal processing that uses practical bounded-input bounded-output (BIBO) stable recursive filters implemented in the spatially-discrete temporally-continuous (SDTC) domain, as shown in Fig. 1. The idea is to exploit 3-D spatio-temporal noise-shaping to improve the effective resolution (as quantified using ENOB) of the ADCs used to digitize 2-D antenna arrays without relying on conventional noise-shaping solutions based on temporal oversampling. The proposed 3-D signal processing algorithm replaces the N^2 conventional ADCs required to digitize an $N \times N$ 2-D antenna array with a single multi-port analog-to-digital converter (ADC) that utilizes noise-shaping in the spatial domain. Although two-dimensional (2-D) algorithms have been explored in the past [4]–[6] and also analogously extended to 3-D [10],

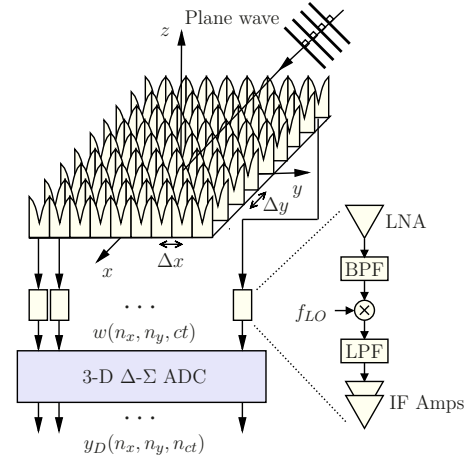


Fig. 1. Plane wave signals received by a spatially-oversampled antenna array are processed through an N^2 -port ADC with spatio-temporal noise shaping.

the 3-D case for rectangular/square arrays is actually not straightforward due to theoretical difficulties in synthesizing practical BIBO stable 3-D feedback loops that possess the necessary 3-D frequency response shapes for signal enhancement and noise shaping while maintaining stability.

This paper summarizes an extensive theoretical effort towards the necessary 3-D filter synthesis that bridges the gap between 2-D (linear array) and 3-D (rectangular/square array) space-time. The proposed work is a significant improvement over [10], in which the transfer functions were not fully confirmed for 3-D noise-shaping requirements but were the only possible theoretical developments available at that time.

II. PLANE WAVE SPECTRA FOR 2-D RECEIVE ARRAYS

Consider a four-dimensional (4-D) propagating far-field electromagnetic plane wave $w_{4C}(x, y, z, ct)$ having azimuth and elevation angles (ϕ, θ) as shown in Fig. 2(a), where $(x, y, z) \in \mathbb{R}^3$ are the spatial dimensions, $t \in \mathbb{R}$ is the time, and c is the speed of a plane wave. The spatial direction of arrival (DOA) is given by the direction cosine vector $[\alpha_x, \alpha_y, \alpha_z]^T$, where $\alpha_x = \cos \phi \cos \theta$, $\alpha_y = \sin \phi \cos \theta$ and $\alpha_z = \sin \theta$ [11, ch. 2], [12, ch. 6]. The direction cosines defined in the 4-D space-time (x, y, z, ct) are given by $\beta_v = \frac{\alpha_v}{\sqrt{\alpha_x^2 + \alpha_y^2 + \alpha_z^2 + \alpha_{ct}^2}}$ where $\alpha_{ct} = 1$ and $v \in \{x, y, z, ct\}$.

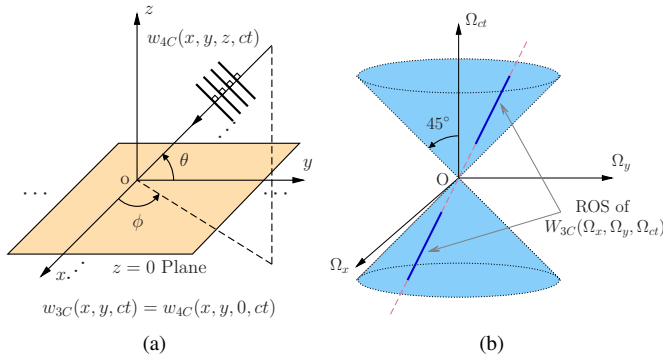


Fig. 2. (a) A 4-D plane wave received by an array surface; (b) the ROS of 3-D plane waves in the continuous spatio-temporal frequency domain.

We assume that the wave is received by a planar array surface constrained to the $z = 0$ plane. Therefore, the 4-D plane wave $w_{4C}(x, y, z, ct)$ reduces to a 3-D plane wave $w_{3C}(x, y, ct)$ for which the 3-D spatio-temporal direction cosines are described by $\beta_v = \frac{\alpha_v}{\sqrt{\alpha_x^2 + \alpha_y^2 + \alpha_z^2 + \alpha_{ct}^2}}$, where $\alpha_{ct} = 1$ and $v \in \{x, y, ct\}$. In this case, broadside incidence reduces the direction cosines to the vector $[0, 0, 1]^T$. The extreme end-fire waves having DOAs $(\phi, 0)$ are circularly symmetric around the array, all corresponding to 3-D spatio-temporal direction cosines of the vector form $[\cos \phi, \sin \phi, 1]^T / \sqrt{2}$.

The region of support (ROS) of a function is defined as the region of the domain where the function is not defined to be zero-valued. The 3-D frequency domain ROS of a propagating plane-wave lies on a straight line passing through the origin of the 3-D continuous spatio-temporal frequency domain $(\Omega_x, \Omega_y, \Omega_{ct}) \in \mathbb{R}^3$ [13]. For example, the ROS of a wideband temporally band-pass plane wave consists of two straight-line segments as shown in Fig. 2(b). The length of the straight-line segment is determined by the temporal bandwidths of the plane wave, and the orientation is determined by the vector given by the 3-D spatio-temporal domain direction of propagation $\beta_v = \frac{\alpha_v}{\sqrt{\alpha_x^2 + \alpha_y^2 + \alpha_z^2 + \alpha_{ct}^2}}$ where $\alpha_{ct} = 1$ and $v \in \{x, y, ct\}$ [13], [14]. The set of all possible propagating plane-waves have combined ROS within the 3-D double-cone shaped region given by $\Omega_x^2 + \Omega_y^2 = \Omega_{ct}^2$ [14], [15]. This region, shown in Fig. 2(b), for the case of propagating plane waves in free space, is the 3-D Fourier domain representation of Einstein's Causality Light Cone, which was first proposed in the Special Theory of Relativity [16].

The spatial sampling of such propagating waves using an array of antennas requires the incident signals to be strictly bandlimited in order to prevent spatio-temporal aliasing. Let the maximum temporal frequency component be $\Omega_{ct} = \Omega_m$. Then, the inter-antenna spacing needs to be selected as $\Delta x = \Delta y \leq \lambda_m/2$, where λ_m is the wavelength corresponding to the frequency Ω_m . For critical sampling, $\Delta x = \Delta y = \lambda_m/2$. The introduction of a uniform square grid of antennas (ideally, point antennas) converts the incident plane waves into a 3-D signal that is discrete in the spatial dimensions but continuous in time. Let the 3-D SDTC signal be defined as $w(n_x, n_y, ct) \equiv w_{3C}(n_x \Delta x, n_y \Delta y, ct)$, where $w_{3C}(x, y, ct)$

is the spatio-temporal plane wave received at the array plane given by $z = 0$. Given that the antennas contain signals that are in the continuous temporal domain, the corresponding ROS is periodic along the 2-D spatial-frequency variables ω_x and ω_y ($\omega_i = \Omega_i \Delta i$, where $i \in \{x, y\}$) but non-periodic and bandlimited along the temporal-frequency variable Ω_{ct} in the 3-D SDTC frequency domain $(\omega_x, \omega_y, \Omega_{ct}) \in \mathbb{R}^3$ [13]. When critical sampling is employed on the spatial dimensions, the combined ROS of all possible incident plane waves pertain to a double-cone having its axis along the Ω_{ct} axis and a half-cone angle of 45° inside the principal Nyquist square cuboid \mathcal{N}_{3S} ($-\pi \leq \omega_x, \omega_y < \pi$ and $-\infty < \Omega_{ct} < \infty$) in the 3-D SDTC frequency domain. In this case, at the highest frequency $\Omega_{ct} = \Omega_m$, the double-cone shaped spectral ROS takes its maximum radius of π . However, spatially over-sampling the array by reducing the inter-antenna spacing by a factor $K_u > 1$ causes the maximum radius of the ROS to decrease to π/K_u .

III. THREE-DIMENSIONAL Δ - Σ ADC NOISE-SHAPING

In the previous section, it was established that the spectral ROS of a 3-D spatially-sampled temporally-continuous (i.e., analog) array signal present at the terminals of the receiver antennas are given by a double-cone region in the 3-D SDTC frequency domain. It was also established that the spatially over-sampled double-cone shaped ROSs have a maximum radius of π/K_u at the highest possible frequency of incident waves Ω_m . For emerging 5G and 6G mm-wave wireless communications and radar applications, the carrier frequency Ω_c can be much greater than than the bandwidth B of the signal of interest. For example, carrier frequencies in the emerging 140 GHz band are typically modulated with a temporal bandwidth less than 2 GHz. The band-pass nature of such incident plane waves allows innovative signal processing algorithms that exploit the double-cone shaped 3-D SDTC frequency domain ROS of the incident plane waves. When $B \ll \Omega_c$, the spectral ROS of a 3-D band-pass plane wave, shown in Fig. 3(a), essentially reduces to two very-short straight-line segments. In this case, a large fraction of the double-cone 3-D spectral ROS is empty (i.e., zero-valued), resulting a double band-pass cone region, as shown in Fig.3(a).

Given that a typical mm-wave or sub-THz array receiver employs highly band-pass signals whose $B \ll \Omega_c$, this allows either i) down-conversion to intermediate frequencies or baseband prior to digitization, or ii) band-pass sampling to achieve both down-conversion and digitization in a single step at the cost of higher noise levels due to noise-folding (a result of temporal aliasing). For example, consider the set of incident waves occupying the band $[\Omega_m - B, \Omega_m]$ with a carrier frequency $\Omega_c = \Omega_m - \frac{B}{2}$. Following down-conversion to an intermediate-frequency (IF) band (with a center frequency of $B/2$), the 3-D SDTC frequency domain ROS now takes a double-conic shape as shown in Fig. 3(b). For typical narrowband signals for which $B \ll \Omega_c$, the double-conic shape appears approximately cylindrical for all practical purposes. The radius of this double-conic 3-D ROS remains

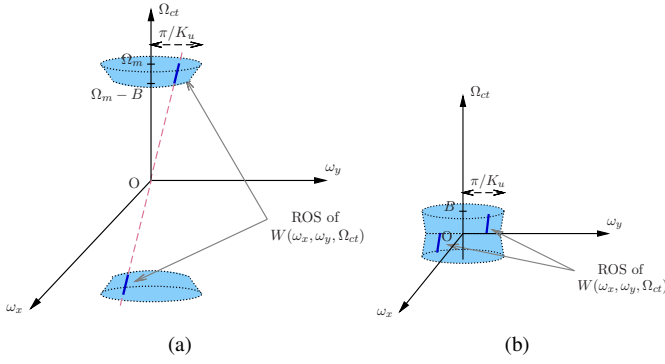


Fig. 3. (a) The ROS of the spectrum of a narrowband plane wave in the 3-D SDTC frequency domain; (b) the ROS after down-conversion to an IF band with a center frequency $B/2$.

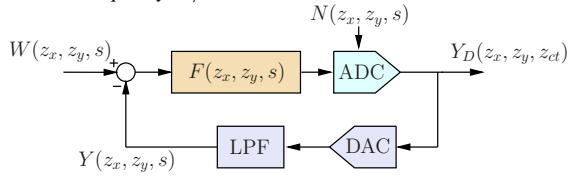


Fig. 4. The proposed three-dimensional noise shaping system.

at π/K_u despite temporal down-conversion. Furthermore, note that the signal is wideband after down-conversion.

Let Φ_{dc} denote the 3-D double-conic ROS of the down-converted signal prior to digitization and $\bar{\Phi}_{dc}$ be the part of the 3-D frequency domain which lies outside the double-conic ROS inside \mathcal{N}_{3S} . We propose a 3-D Δ - Σ spatio-temporal feedback system, shown in Fig. 4, that provides ADC noise shaping such that the signal of interest having ROS Φ_{dc} is subject to a 2-D spatial passband function $H_p(z_x, z_y, s)$ that approximates Φ_{dc} while noise and distortion is shaped into the region given ideally by $\bar{\Phi}_{dc}$, which is achieved via the spatial noise-shaping function $H_n(z_x, z_y, s) = 1 - H_p(z_x, z_y, s)$.

A. Design and Realization of $F(z_x, z_y, s)$

In the proposed 3-D ADC noise-shaping system, shown in Fig. 4, the incident SDTC array signal $w(n_x, n_y, ct) \Leftrightarrow W(z_x, z_y, s)$ is subject to the 3-D transfer function

$$H_p(z_x, z_y, s) = \frac{F(z_x, z_y, s)}{1 + F(z_x, z_y, s)}, \quad (1)$$

while internal 3-D spatio-temporal noise and distortion $n(n_x, n_y, ct) \Leftrightarrow N(z_x, z_y, s)$ is subject to the shaping function

$$H_n(z_x, z_y, s) = \frac{1}{1 + F(z_x, z_y, s)}. \quad (2)$$

We propose the forward function $F(z_x, z_y, s)$, which is ideally independent of the temporal frequency Ω_{ct} , as

$$F(z_x, z_y, s) = \frac{a(1 + z_x^{-1} + z_y^{-1} + z_x^{-1}z_y^{-1})}{1 + b_1(z_x^{-1} + z_y^{-1}) + b_2z_x^{-1}z_y^{-1}}, \quad (3)$$

where, $a = \alpha^2/(1 - \alpha^2)$, $b_1 = (\beta - \alpha^2)/(1 - \alpha^2)$ and $b_2 = (\beta^2 - \alpha^2)/(1 - \alpha^2)$. Here, α and β are defined using a first-order low-pass Butterworth filter of which the transfer function is given by $H(z) = \frac{\alpha(1+z^{-1})}{1+\beta z^{-1}}$ [17, ch. 10].

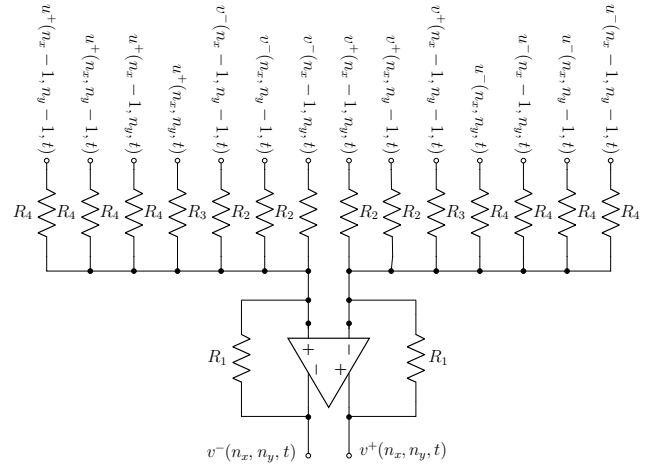


Fig. 5. Realization of a module of $F(z_x, z_y, s)$, where $u(n_x, n_y, t)$ and $v(n_x, n_y, t)$ are the input and the output, respectively.

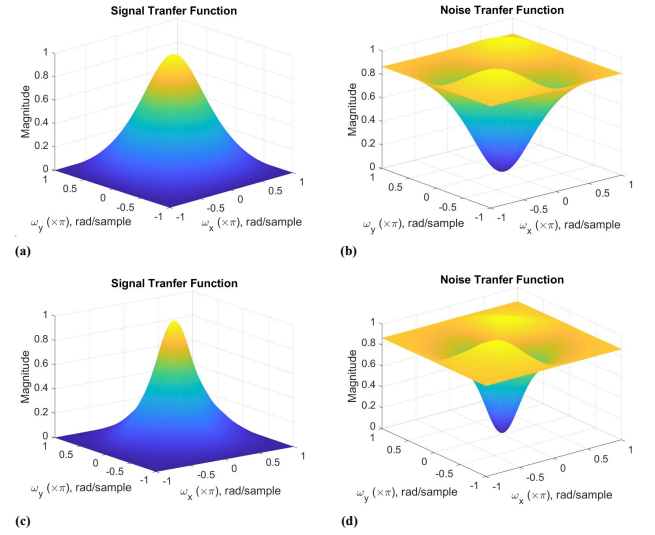


Fig. 6. MATLAB simulation results for the magnitude frequency responses of (a) the signal transfer function $H_p(z_x, z_y, s)$ and (b) noise transfer function $H_n(z_x, z_y, s)$, assuming $K_u = 3$. (c)-(d) Same as (a)-(b), but for $K_u = 5$.

The system $F(z_x, z_y, s)$ can be realized using N^2 operational amplifiers for an $N \times N$ antenna array, resulting in N^2 similar modules. The realization of one such module is shown in Fig. 5, assuming $a, b_1, b_2 > 0$. In this case, $a = \frac{R_1}{R_4}$, $b_1 = \frac{R_1}{R_2}$, and $b_2 = \frac{R_1}{R_3}$; $v^+(n_x, n_y, t)$ and $v^-(n_x, n_y, t)$ refer to the outputs of the differential op-amp; and $u^+(n_x, n_y, t)$ and $u^-(n_x, n_y, t)$ are the differential inputs.

B. Dominant-Pole 3-D Transfer Functions

Although the spatial 2-D noise shaping function was developed as a purely spatial operation, real-world electronics uses amplifiers with finite gains and dominant-pole frequency responses to ensure stability [18]. Let the dominant pole frequency be at $B_{\lambda 1}$ for the outer feedback loop. We therefore modify the spatial noise shaping operation using a dominant pole response for the active circuitry [19] to obtain the

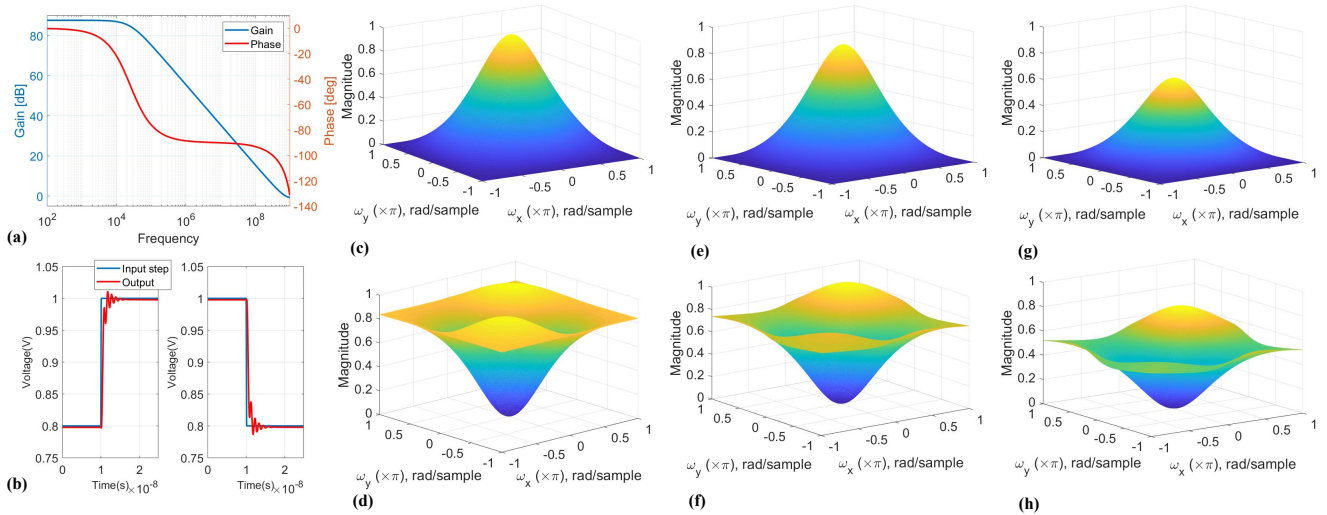


Fig. 7. Op-amp simulations: (a) open-loop gain and phase, (b) step responses. Cadence Spectre simulation results for the magnitude frequency responses of signal and noise transfer functions at a temporal frequency of (c) and (d) DC, (e) and (f) 25 MHz, and (g) and (h) 50 MHz, when $K_u = 3$.

modified transfer functions

$$H_{p,dp}(z_x, z_y, s) = \frac{F_{dp}(z_x, z_y, s)}{1 + \frac{F_{dp}(z_x, z_y, s)}{1 + s/B_{\lambda 1}}}, \quad (4)$$

and

$$H_{n,dp}(z_x, z_y, s) = \frac{1}{1 + \frac{F_{dp}(z_x, z_y, s)}{1 + s/B_{\lambda 1}}} \quad (5)$$

where $F_{dp}(z_x, z_y, s)$ is the 3-D forward function, which itself is not subject to a dominant pole response. Let the dominant pole response for the forward function be $B_{\lambda 2}$. Therefore, the dominant pole response of the forward function is modeled as

$$F_{dp}(z_x, z_y, s) = \frac{a(1 + z_x^{-1} + z_y^{-1} + z_x^{-1}z_y^{-1})}{1 + \frac{b_1(z_x^{-1} + z_y^{-1}) + b_2z_x^{-1}z_y^{-1}}{1 + s/B_{\lambda 2}}} \cdot \frac{1}{1 + s/B_{\lambda 2}}. \quad (6)$$

IV. SIMULATION RESULTS

We consider two examples with spatial oversampling factors $K_u = 3$ and $K_u = 5$. In these cases, the cutoff frequency ω_c of the first-order low-pass Butterworth filter is selected as 0.33π rad/sample and 0.2π rad/sample, respectively. For the case $K_u = 3$, $\alpha = 0.3632$ and $\beta = -0.2736$, and for the case $K_u = 5$, $\alpha = 0.2452$ and $\beta = -0.5095$. MATLAB simulation results for the magnitude frequency responses of the signal transfer function $H_p(z_x, z_y, s)$ and the noise transfer function $H_n(z_x, z_y, s)$ are shown in Fig. 6. It can be clearly seen that the frequency responses of $H_p(z_x, z_y, s)$ and $H_n(z_x, z_y, s)$ provide low-pass and high-pass rotationally (approximately circularly) symmetric frequency responses, respectively, as required for noise and distortion shaping at IF (or baseband) across a square/rectangular array.

A. Analog-Circuit Realization of 3-D Transfer-Functions

In order to verify the practical realization of the proposed 3-D filters, the 3-D noise shaping system shown in Fig. 4 was designed using an array of 8×8 operational amplifiers. The

system $F(z_x, z_y, s)$ was realized as in Fig. 5. For simplicity, ADCs and digital-to-analog converters (DACs) were modeled as white Gaussian noise sources. In this case, other distributions such as uniform distribution, can also be used for modeling. The fully-differential op-amp used in the circuit was designed using TSMC 180 nm CMOS technology [20]. This is a two-stage design with a gain bandwidth product of 750 MHz and a phase margin of 60° . The differential open-loop DC gain of the op-amp is ~ 87 dB and the slew rate is 350 V/ μ s. Simulated gain and phase characteristics of the op-amp and its small-signal step responses are shown in Figs. 7 (a) and (b) respectively.

System-level transient simulations were conducted using Cadence Spectre. For this purpose, the circuit was excited with a 50 mV input pulse of width 10 ns, and the output of each op-amp was recorded at a sampling rate of 1 ns. The resulting 3-D signal was converted to the 3-D discrete frequency domain using a 3-D Fourier transform. Fig. 7 (c)-(h) shows the simulated spatial frequency responses for the signal transfer function $H_p(z_x, z_y, s)$ and noise transfer function $H_n(z_x, z_y, s)$ at different temporal frequencies from DC to 50 MHz when $K_u = 3$. In each case, the frequency responses obtained from circuit simulations are similar to the MATLAB simulation results, which verifies the proposed approach.

V. CONCLUSIONS

This paper has described a 3-D spatio-temporal noise shaping method for increasing the effective resolution of N^2 -port ADCs that digitize plane waves received by $N \times N$ 2-D square/rectangular antenna arrays. The method was implemented using high-speed op-amps in 180 nm CMOS, and its performance verified (in simulation) for temporal frequencies up to 50 MHz. Future work will focus on implementing the system with ADC/DAC circuits and improving the useful ADC bandwidth by further increasing the gain bandwidth product of the op-amps; this will be followed by layout, fabrication, and experimental verification.

REFERENCES

- [1] D. P. Scholnik, J. O. Coleman, D. Bowling, and M. Neel, "Spatio-temporal delta-sigma modulation for shared wideband transmit arrays," in *Proceedings of the 2004 IEEE Radar Conference (IEEE Cat. No. 04CH37509)*. IEEE, 2004, pp. 85–90.
- [2] S. Handagala, A. Madanayake, L. Belostotski, and L. T. Bruton, "Delta-sigma noise shaping in 2D spacetime for uniform linear aperture array receivers," in *2016 Moratuwa Engineering Research Conference (MERCon)*, April 2016, pp. 114–119.
- [3] R. M. Corey and A. C. Singer, "Spatial sigma-delta signal acquisition for wideband beamforming arrays," in *WSA 2016; 20th International ITG Workshop on Smart Antennas*. VDE, 2016, pp. 1–7.
- [4] Y. Wang, S. Handagala, A. Madanayake, L. Belostotski, and S. Mandal, "N-port LNAs for mmw array processors using 2-D spatio-temporal $\Delta - \Sigma$ noise-shaping," in *2017 IEEE 60th International Midwest Symposium on Circuits and Systems (MWSCAS)*, Aug 2017, pp. 1473–1476.
- [5] A. Nikoofard, J. Liang, M. Twieg, S. Handagala, A. Madanayake, L. Belostotski, and S. Mandal, "Low-complexity N-port ADCs using 2-D $\Delta - \Sigma$ noise-shaping for N-element array receivers," in *2017 IEEE 60th International Midwest Symposium on Circuits and Systems (MWSCAS)*, Aug 2017, pp. 301–304.
- [6] Y. Wang, J. Liang, S. Handagala, A. Madanayake, and S. Mandal, " $\Delta - \Sigma$ noise-shaping in 2-D space-time for wideband antenna array receivers," *IEEE Transactions on Circuits and Systems I: Regular Papers*, vol. 66, no. 2, pp. 569–582, Feb 2019.
- [7] H. Pirzadeh, G. Seco-Granados, S. Rao, and A. L. Swindlehurst, "Spectral efficiency of one-bit sigma-delta massive MIMO," *arXiv preprint arXiv:1910.05491*, 2019.
- [8] A. Madanayake, N. Akram, S. Mandal, J. Liang, and L. Belostotski, "Improving adc figure-of-merit in wideband antenna array receivers using multidimensional space-time delta-sigma multiport circuits," in *2017 10th International Workshop on Multidimensional (nD) Systems (nDS)*, Sep. 2017, pp. 1–6.
- [9] S. Rao, A. L. Swindlehurst, and H. Pirzadeh, "Massive MIMO channel estimation with 1-bit spatial sigma-delta ADCs," in *ICASSP 2019-2019 IEEE International Conference on Acoustics, Speech and Signal Processing (ICASSP)*. IEEE, 2019, pp. 4484–4488.
- [10] Y. Wang, J. Liang, A. Madanayake, L. Belostotski, and S. Mandal, "Delta-Sigma noise-shaping in 3D space-time for 2-D wideband antenna array receivers," *Springer Multidimensional Systems and Signal Processing (MSSP)*, 2018, Accepted.
- [11] H. L. Van Trees, *Optimum Array Processing: Part IV of Detection, Estimation, and Modulation Theory*. NY: John Wiley & Sons, 2002.
- [12] D. E. Dudgeon and R. M. Mersereau, *Multidimensional Digital Signal Processing*. Englewood Cliffs, NJ: Prentice-Hall, 1984.
- [13] L. T. Bruton and N. R. Bartley, "Three-dimensional image processing using the concept of network resonance," *IEEE Trans. Circuits Syst.*, vol. CAS-32, no. 7, pp. 664–672, Jul. 1985.
- [14] L. T. Bruton, "Three-dimensional cone filter banks," *IEEE Trans. Circuits Syst. I*, vol. 50, no. 2, pp. 208–216, Feb. 2003.
- [15] T. K. Gunaratne and L. T. Bruton, "Broadband beamforming of dense aperture array (DAA) and focal plane array (FPA) signals using 3D spatio-temporal filters for applications in aperture synthesis radio astronomy," *Multidim. Syst. Signal Process.*, vol. 22, no. 1–3, pp. 213–236, Mar. 2011.
- [16] A. Einstein, *Relativity: The Special and General Theory*. NY: Henry Holt & Company, 1920.
- [17] A. Antoniou, *Digital Signal Processing: Signals, Systems and Filters*. NY: McGraw-Hill, 2006.
- [18] L. Zhang, A. Natarajan, and H. Krishnaswamy, "Scalable spatial notch suppression in spatio-spectral-filtering MIMO receiver arrays for digital beamforming," *IEEE Journal of Solid-State Circuits*, vol. 51, no. 12, pp. 3152–3166, Dec 2016.
- [19] B. Mazhari, "On the estimation of frequency response in amplifiers using Miller's theorem," *IEEE Transactions on Education*, vol. 48, no. 3, pp. 559–561, Aug 2005.
- [20] S. Shekhar, J. S. Walling, and D. J. Allstot, "Bandwidth extension techniques for CMOS amplifiers," *IEEE Journal of Solid-State Circuits*, vol. 41, no. 11, pp. 2424–2439, Nov 2006.